ChemComm

ROYAL SOCIETY OF CHEMISTRY

COMMUNICATION

View Article Online
View Journal | View Issue

Cite this: *Chem. Commun.*, 2025, **61**, 520

Received 8th August 2024,
Accepted 22nd November 2024

DOI: 10.1039/d4cc04050c

rsc.li/chemcomm

Electrochemical aldehyde hydrogenation: probing the inner-sphere strategy with nickel-bipyridine complexes†

Gabriel Durin, ‡[ab] Mijung Lee, ‡[a] Martina A. Pogany, ‡[a] Christian Kahl,[a] Thomas Weyhermüller,[a] Walter Leitner[ac] and Nicolas Kaeffer *[a]

Developing electrohydrogenation routes for organics is crucial in synthesis electrification. Herein, we examine the electrocatalytic hydrogenation of aldehydes through an inner-sphere mechanism at a nickel-bipyridine complex. An (electro)reduction triggers the coordination of the aldehyde into a key nickeloxirane species, which affords hydrogenation products by stoichiometric protonations. Turnover yet remains challenging with acids suitable for electrocatalytic conditions due to sluggish proton transfers, which we probed by combined reactivity and computational studies.

The electrification of synthetic processes is empowering the use of renewable and sustainable resources in chemistry.[1–5] This virtuous approach is often propelled by electrocatalysis to incorporate energy efficiency and selectivity. A key to the rational development of these electrocatalytic systems is the decoding of the mechanisms involved. The well-defined nature of molecular complexes facilitates access to mechanistic information. This strategy has led to molecular electrocatalytic systems for the hydrogenation of organic multiple bonds.[6–17] In contrast to CO_2 reduction, the electrocatalytic hydrogenation (ECH) of organic carbonyls with molecular complexes remains largely under-explored.[18]

Siewert and co-workers demonstrated the repurposing of {Mn(bpy)}-type hydrogenation electrocatalysts from CO_2 to organic carbonyls, including aliphatic aldehydes,[15,16] while Waymouth and co-workers addressed the challenging ECH of benzaldehyde using a Mo Shvo-type complex[14] (Scheme 1). These systems perform hydrogenation through the evolution of a metal hydride that is transferred to the electrophilic C–O carbon.

In our exploration of electrocatalyzed synthesis, we recently employed the coordination ability of nickel-bipyridine complexes to achieve alkyne ECH through successive electron and proton transfers, bypassing metal hydride intermediates.[19,20] This approach exploits hydride-free selective pathways that are at odds with catalysis in thermal hydrogenation and reported ECHs. Herein, we investigate the challenges in transposing the hydride-free strategy from the hydrogenation of C–C multiple bonds to that of C–O bonds (Scheme 1).

Knowing that [Ni(bpy)(BzO)$_2$] (**1**) is a hydrogenation electrocatalyst for alkyne substrates,[20] we aimed at probing this complex for carbonyl substrates.

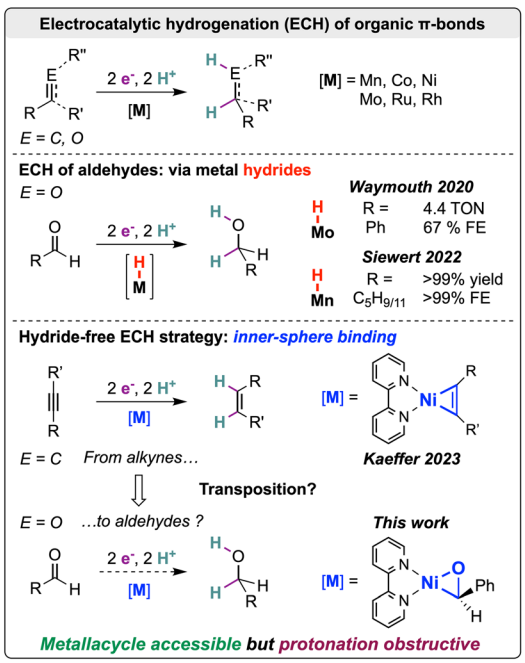

Scheme 1 Electrocatalytic hydrogenation of C–O and C–C multiple bonds by molecular complexes, including nickel-bipyridine complexes.

[a] Max Planck Institute for Chemical Energy Conversion, Stiftstrasse 34-36, 45470 Mülheim an der Ruhr, Germany. E-mail: nicolas.kaeffer@cec.mpg.de
[b] Université Grenoble Alpes, DCM, CNRS, 38000 Grenoble, France
[c] Institut für Technische und Makromolekulare Chemie, RWTH Aachen University, Worringerweg 2, 52074 Aachen, Germany

† Electronic supplementary information (ESI) available. CCDC 2374778. For ESI and crystallographic data in CIF or other electronic format see DOI: https://doi.org/10.1039/d4cc04050c

‡ These authors contributed equally to this work.

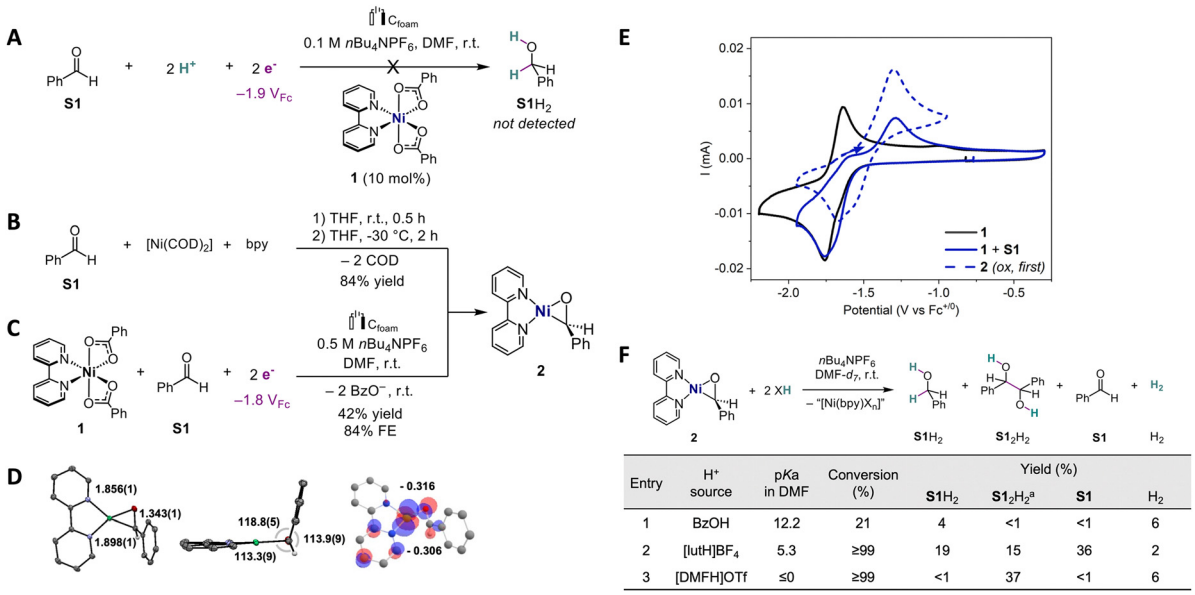

Entry	H+ source	pKa in DMF	Conversion (%)	Yield (%)			
				S1H2	S1$_2$H$_2$[a]	S1	H$_2$
1	BzOH	12.2	21	4	<1	<1	6
2	[lutH]BF$_4$	5.3	≥99	19	15	36	2
3	[DMFH]OTf	≤0	≥99	<1	37	<1	6

Scheme 2 (A) Electrocatalytic attempt using **1** (1 mM), **S1** (10 mM), and BzOH (22 mM) after passing 8.5C (approximately 2e$^-$/**S1**). (B) Synthesis of **2** from [Ni(COD)$_2$]. (C) Electrosynthesis of **2** from **1** at E_{app} = −1.80 V$_{Fc}$ (charge = 4.56C; approximately 1e$^-$/**1**). (D) Molecular structure of **2** obtained by XRD (ORTEP; 50% probability; color code: gray: C; purple: N; green: Ni; red: O; white: H) and computed electron density of the HOMO of **2** with Mulliken charges at aldehydic C and O (H atoms omitted for clarity, except aldehydic ones). (E) CVs of **1**, **1** and **S1**, and **2** (1 mM each; 0.1 V s^{-1} scan rate). **F** Protonation reactions starting from **2** (at 30 min). Unless otherwise stated, the supporting electrolyte is DMF 0.1 M *n*Bu$_4$NPF$_6$. [a] Maximum theoretical yield 50%.

However, electrolysis of benzaldehyde (**S1**) in the presence of **1** and benzoic acid (BzOH) as a proton source leads to marginal conversion and no detected hydrogenation product **S1**H$_2$, once approximately 2 electrons were passed per **S1** (Scheme 2A). Varying the solvent (*e.g.*, DMSO, THF) or even the substrate (*p*-MeO-PhCHO) was not productive. Moreover, greater cathodic applied potential (see ESI,† Section S3.4) or higher acidity (*e.g.*, [DMFH]OTf)[21] trigger the direct reduction of **S1** at the electrode, and hence are not compatible with this system.

In the absence of catalysis, it is thus questionable whether a pathway involving a nickelacyclic intermediate, in analogy to the nickelacyclopropene reported for alkyne semi-hydrogenation, is viable in the case of C=O bond hydrogenation. We examined the formation of such species in the case of C–O unsaturations by reacting a 1 : 1 mixture of [Ni(COD)$_2$] (COD = 1,4-cyclooctadiene) and 2,2′-bipyridine with benzaldehyde (**S1**) in THF, inspired by previous studies and our precedents.[20,22,23] The reaction quickly evolves a green precipitate identified after the workup as nickeloxirane [Ni(bpy)(PhCHO)][22–24] (**2**), obtained in 84% yield (Scheme 2B and ESI,† Section S2.1).

The molecular structure was elucidated by single crystal X-ray diffraction (XRD), and indicates a planar geometry for nickeloxirane **2** (Scheme 2D; ESI,† Section S2.4) with a C–O bond length of 1.343 Å, which was quite elongated relative to **S1** (1.210 Å).[25] Moreover, the ^{1}H NMR signature (DMSO-d_6) attributed to the aldehydic hydrogen of **2** is manifested by a broad singlet at 5.05 ppm, in a region typical of benzylic resonances (*vs.* 10.02 ppm in free **S1**). Additionally, the C–O stretching frequency at 1360 cm^{-1} in **2** undergoes a substantial redshift compared to free **S1** (ν(C=O) = 1693 cm^{-1}; see ESI†, Section 2.3). This spectroscopic evidence further reinforces the C–O single-bond characteristic in **2**.

Investigating the voltammetric behavior of **1** shows that the addition of aldehyde **S1** (1 equiv.) triggers the reduction wave at $E_{p,c}$ = −1.76 V$_{Fc}$[20] (V$_{Fc}$ stands for V *vs.* Fc$^{+/0}$) to evolve a shoulder ($E \approx$ −1.70 V$_{Fc}$) and lose its reversibility (Scheme 2E). Most importantly, these changes are accompanied by the buildup of an anodic wave at $E_{p,a}$ = −1.29 V$_{Fc}$, matching that observed for the oxidation of native **2**. These points suggest that **2** can also be formed by reductive electrogeneration from **1** and **S1**. Bulk reductive electrolysis of a mixture of **1** and **S1** at E_{app} = −1.80 V$_{Fc}$ (**1**/**S1** 1 : 1 ratio, approximately 1e$^-$/**1** at saturation) (Scheme 2C) further confirms the electrogeneration of **2** in 42% yield and 84% faradaic efficiency, as revealed by the characteristic voltammetric and ^{1}H NMR signatures (ESI,† Section S4.4).

While these results demonstrate the binding and activation of **S1** in nickelacyclic species **2**, including under electroreductive conditions, protonation is required to release the genated product and induce turnover. After 30 min, addition of 2 equivalents of BzOH (pK_a 12.2 in DMF[26]) to **2** dissolved in DMF-d_7 and *n*Bu$_4$NPF$_6$ 20 mM (r.t.) affords 21% conversion of **2** and a 4% yield in **S1**H$_2$ with H$_2$ as a byproduct (6% yield) (Scheme 2F; entry 1). Extending the reaction time to 24 h leads to full conversion and **S1**H$_2$ in 17% yield (see ESI,† Section S4.1 for additional details). These results indicate the slow reactivity of BzOH with **2**, leading to hydrogenation into **S1**H$_2$ and the hydrogen evolution reaction (HER). The latter reactivity suggests the formation of nickel hydride species, while the former can also proceed by protonations of the metallacycle as observed with alkynes.[20]

To determine if stronger acids would accelerate the reaction or promote one reaction pattern over the other, we tested 2,6-lutidinium (lutH$^+$ pK_a 5.3 in DMF;[27,28] Scheme 2F; entry 2).

After 30 min, **2** is fully converted and affords **S1**H_2 in 19% yield and low hydrogen evolution (2%). It is worth noting two additional points. First, the pinacol coupling product hydrobenzoin (**S1**$_2H_2$) is detected in substantial yields (15%). Second, significant amounts of unreacted **S1** are released (36%), which indicates the displacement of that substrate from the Ni center.

We surmise that this expulsion is induced by the coordination of the proton source at Ni, potentially leading to $[Ni(bpy)(lut)(H)]^+$, a hydride species. That hypothesis is reinforced by the observation of a ^{1}H NMR signal at −21.74 ppm (Fig. S14, ESI†), which was attributed to such Ni–H hydride compounds by comparison with literature data.[29,30] Evidence consisting of the concomitant observation of the Ni–H species and free **S1** indicates that this hydride is not highly reactive towards the aldehyde. In the case of the more acidic $DMFH^+$ ($pK_a \leq 0$ in DMF[26,28]), the selectivity in **S1**-derived products is now fully switched to **S1**$_2H_2$ (Scheme 2F; entry 3), while Ni–H is also detected (Fig. S14, ESI†). The increased selectivity for the product **S1**$_2H_2$ when Ni–H is detected suggests $1e^-/1H^+$ reactivity[31] of these hydrides.

We further explored the conditions for hydrogenation (see ESI,† Sections S4.1–S4.3). With **2**, the use of alternative Brønsted acids does not increase yields in hydrogenated products, and Lewis acids do not afford hydrogenation. Regarding ligands, the more electron-poor 4,4-bis(trifluoromethyl)-2,2′-bipyridine fails to generate an aldehyde adduct, but a nickeloxirane forms when electron-donating 4,4-bis(methoxy)-2,2′-bipyridine is used, which in turn leads to similar protonation results. The combination of **2** and $lutH^+$ provides the highest yield of **S1**H_2.

These results indicate that the (electro)reductive generation of the nickelacyclic species **2** from **S1** is feasible, but subsequent reactivity is undermined by competing hydride formation or slow protonation. While $lutH^+$ or $DMFH^+$ afford fast conversion of **2** into the hydrogenation products of **S1**, these proton sources are too acidic for the investigated electrocatalytic potentials. In contrast, the less acidic BzOH appropriate to ECH of alkyne leads to sluggish reactivity.

To further uncover the mechanistic limitations and the underlying distinctions of the operating alkyne ECH case, we employed DFT calculations (Scheme 3). We considered an initiation from **1** by 2-electron reduction associated with the release of a benzoate ligand, leading to **I1** as previously described,[20] and used this as the reference entry point. The binding of **S1** to **I1** by associative displacement of BzO^- is kinetically facile ($TS_{I1\text{-}2}$ at +2.8 kcal mol^{-1}) and highly favored, leading to nickeloxirane **2** as the most stable computed intermediate (ΔG = −23.8 kcal mol^{-1}). We note that, aside from being a relevant species by electrochemical access, **2** is also the starting material in our stoichiometric experiments. We then investigated protonation at the substrate sites in **2**, namely at the C or the O atom in the nickelacycle.

There is a reachable transition state (TS) for the calculated O-protonation ($TS_{2\text{-}I2}$ at $\Delta\Delta G^{\ddagger}$ = +14.7 kcal mol^{-1}), but the formation of the nickel-alkyl species **I2** is endergonic ($\Delta\Delta G$ = +5.4 kcal mol^{-1}). Furthermore, this intermediate appears unproductive because neither protonation nor isomerization seems plausible (see ESI,† Section S5.2). C-protonation is computed to afford a relatively stable benzolate complex **I3** (ΔG = −21.3 kcal mol^{-1}), from which a second O-protonation is feasible to release the desired product **S1**H_2. However, the initial C-protonation is hindered by high energy cost at $TS_{2\text{-}I3}$ ($\Delta\Delta G^{\ddagger}$ = +26.1 kcal mol^{-1}). It was noted that β-H elimination, which would have contributed to the hydride pathway (HER) from **I2** and **I3**, is unlikely, with TSs >27 kcal mol^{-1}. Consequently, the computational results support the difficulty of protonations of **2** by BzOH and, within computational uncertainty, are close to feasibility limits at RT (>23 kcal mol^{-1}), further corroborating the slow and understoichiometric evolution of **S1**H_2 observed in chemical conditions.

We next turned to the formation of hydride species to trace the HER with our system. The electrogeneration of **I1** from

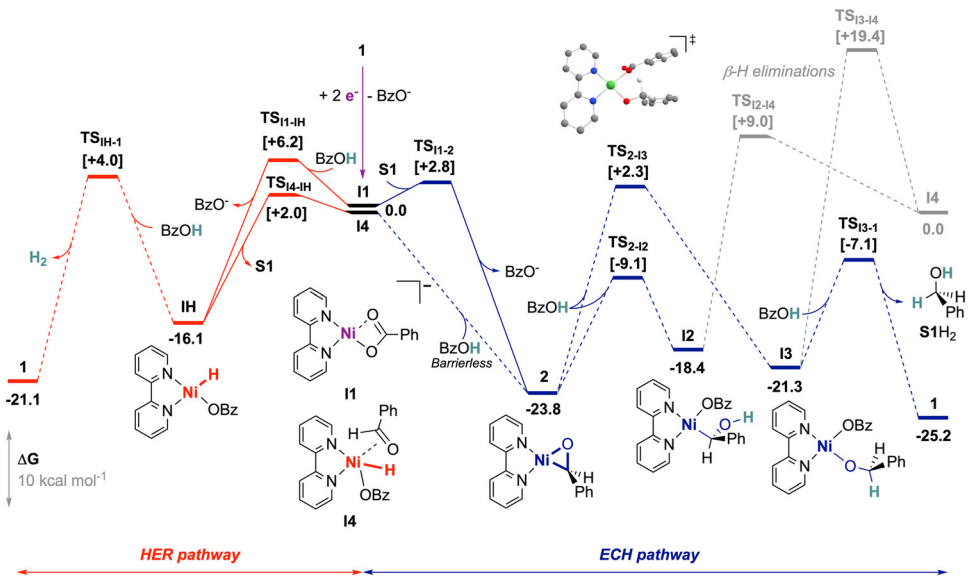

Scheme 3 Computed HER (red)[20] and ECH (blue) pathways at the PBE-D3/6-311+G(d,p) level of theory using the CPCM model to account for the solvent effect of DMF.

precatalyst **1** can lead to a slow HER *via* the hydride complex **IH**, as previously described.[20] However, **I1** is not relevant in stoichiometric experiments with **2**, yet it produces H_2. In that case, we found that the oxidative addition of BzOH at **2** leads to hydride **I4** without barriers, thus restoring the occurrence of the HER. The span of that pathway is relatively high (+25.8 kcal mol^{-1}), but it cannot be fully discarded within the uncertainty of the calculations, and hence can possibly account for H_2 produced.

For the formation of the hydrobenzoin **S1**$_2$H$_2$, a radical pathway resulting from the homolytic cleavage of the Ni–C bond of **I2** (BDE = 34.6 kcal mol^{-1}) seems reasonable. Another pathway involving ring expansion by addition of **S1** to **2** proved to be too high in energy (> 29 kcal mol^{-1}; see ESI,† Section S5.2).

S1 binding into **2** and **IH** hydride generation are expected to rapidly occur from **I1**, with respective computed TSs of 2.8 and 6.2 kcal mol^{-1}, but **2** is strongly stabilized *versus* **IH** by 7.7 kcal mol^{-1}. The accumulation of the nickelaoxirane is therefore plausible in the hypothesis of slow subsequent kinetics supported by the elevated spans. In this regard, in the voltammetry of **1** recorded with excess BzOH, the addition of 1 equivalent of **S1** restores the electrochemical signature of **2** (Fig. S9, ESI†). This displacement of the electrochemical systems towards **2** even in the presence of BzOH corroborates the thermodynamic preference of the nickelaoxirane *versus* the hydride species and further shows that **S1** inhibits the HER. We note that this relative stability with respect to **IH** is lower for nickeloxirane as compared to nickelacyclopropene[20] (ΔG(metallacycle → IH) = 7.7 *vs.* 13.9 kcal mol^{-1}), which supports a more accessible nickel hydride in the case of aldehyde as a substrate.

In summary, in an approach to transpose a hydride-free electrocatalytic hydrogenation from C–C to C–O π-bonds, we demonstrated the successful (electro)generation of a key nickeloxirane species, leading to hydrogenation products by stoichiometric protonation. However, identifying efficient electrocatalytic conditions remains challenging. We determined that inner-sphere substrate binding is preferred over hydride formation, but subsequent protonations of the nickelacyclic species are obstructive. These findings will guide further molecular catalysis for carbonyl electrohydrogenation.

The authors gratefully acknowledge basic support from the Max Planck Society and the RWTH Aachen University. They thank Annika Gurowski, Alina Jakubowski and Justus Werkmeister for assistance with analytical measurements. Open Access funding provided by the Max Planck Society.

Data availability

The data supporting this article are included as part of the ESI.† The crystallographic data for **2** have been deposited at the CCDC under number 2374778.

Conflicts of interest

There are no conflicts to declare.

Notes and references

1 A. Wiebe, T. Gieshoff, S. Mohle, E. Rodrigo, M. Zirbes and S. R. Waldvogel, *Angew. Chem., Int. Ed.*, 2018, **57**, 5594–5619.
2 N. Kaeffer and W. Leitner, *JACS Au*, 2022, **2**, 1266–1289.
3 N. von Wolff, O. Rivada-Wheelaghan and D. Tocqueville, *ChemElectroChem*, 2021, **8**, 4019–4027.
4 G. Centi, S. Perathoner, C. Genovese and R. Arrigo, *Chem. Commun.*, 2023, **59**, 3005–3023.
5 Z. Liu, L. Zhang, Z. Ren and J. Zhang, *Chem. – Eur. J.*, 2023, **29**, e202202979.
6 J. Derosa, P. Garrido-Barros and J. C. Peters, *J. Am. Chem. Soc.*, 2021, **143**, 9303–9307.
7 J. Derosa, P. Garrido-Barros, M. Li and J. C. Peters, *J. Am. Chem. Soc.*, 2022, **144**, 20118–20125.
8 S. Gnaim, A. Bauer, H.-J. Zhang, L. Chen, C. Gannett, C. A. Malapit, D. E. Hill, D. Vogt, T. Tang, R. A. Daley, W. Hao, R. Zeng, M. Quertenmont, W. D. Beck, E. Kandahari, J. C. Vantourout, P.-G. Echeverria, H. D. Abruna, D. G. Blackmond, S. D. Minteer, S. E. Reisman, M. S. Sigman and P. S. Baran, *Nature*, 2022, **605**, 687–695.
9 X. Wu, C. N. Gannett, J. Liu, R. Zeng, L. F. T. Novaes, H. Wang, H. D. Abruña and S. Lin, *J. Am. Chem. Soc.*, 2022, **144**, 17783–17791.
10 I. M. F. De Oliveira and J.-C. Moutet, *J. Mol. Catal.*, 1993, **81**, L19–L24.
11 J.-C. Moutet, L. Yao Cho, C. Duboc-Toia, S. Ménage, E. C. Riesgo and R. P. Thummel, *New J. Chem.*, 1999, **23**, 939–944.
12 H. Shimakoshi, Z. Luo, K. Tomita and Y. Hisaeda, *J. Organomet. Chem.*, 2017, **839**, 71–77.
13 M. H. Rønne, D. Cho, M. R. Madsen, J. B. Jakobsen, S. Eom, É. Escoudé, H. C. D. Hammershøj, D. U. Nielsen, S. U. Pedersen, M.-H. Baik, T. Skrydstrup and K. Daasbjerg, *J. Am. Chem. Soc.*, 2020, **142**, 4265–4275.
14 K. C. Armstrong and R. M. Waymouth, *Organometallics*, 2020, **39**, 4415–4419.
15 I. Fokin and I. Siewert, *Chem. – Eur. J.*, 2020, **26**, 14137–14143.
16 I. Fokin, K.-T. Kuessner and I. Siewert, *ACS Catal.*, 2022, **12**, 8632–8640.
17 D. P. Marron, C. M. Galvin, J. M. Dressel and R. M. Waymouth, *J. Am. Chem. Soc.*, 2024, **146**, 17075–17083.
18 G. Durin, N. Kaeffer and W. Leitner, *Curr. Opin. Electrochem.*, 2023, **41**, 101371.
19 M. Y. Lee, C. Kahl, N. Kaeffer and W. Leitner, *JACS Au*, 2022, **2**, 573–578.
20 G. Durin, M. Y. Lee, M. A. Pogany, T. Weyhermuller, N. Kaeffer and W. Leitner, *J. Am. Chem. Soc.*, 2023, **145**, 17103–17111.
21 M. Chandrasekaran, M. Noel and V. Krishnan, *J. Electroanal. Chem.*, 1991, **303**, 185–197.
22 E. Dinjus, I. Gorski, H. Matschiner, E. Uhlig and D. Walther, *Z. Anorg. Allg. Chem.*, 1977, **436**, 39–46.
23 E. Dinjus, H. Langbein and D. Walther, *J. Organomet. Chem.*, 1978, **152**, 229–237.
24 We note that the synthesis of **2** had been previously reported in ref. 23, but with partial characterization (elemental analysis, infrared and ultraviolet-visible spectroscopies).
25 K. B. Borisenko, C. W. Bock and I. Hargittai, *J. Phys. Chem.*, 1996, **100**, 7426–7434.
26 V. Fourmond, P. A. Jacques, M. Fontecave and V. Artero, *Inorg. Chem.*, 2010, **49**, 10338–10347.
27 A. Kütt, S. Tshepelevitsh, J. Saame, M. Lõkov, I. Kaljurand, S. Selberg and I. Leito, *Eur. J. Org. Chem.*, 2021, 1407–1419.
28 L. Sooväli, I. Kaljurand, A. Kütt and I. Leito, *Anal. Chim. Acta*, 2006, **566**, 290–303.
29 J. Breitenfeld, O. Vechorkin, C. Corminboeuf, R. Scopelliti and X. Hu, *Organometallics*, 2010, **29**, 3686–3689.
30 A. K. Ravn, M. B. Johansen and T. Skrydstrup, *Angew. Chem., Int. Ed.*, 2022, **61**, e202112390.
31 M. J. Chalkley, P. Garrido-Barros and J. C. Peters, *Science*, 2020, **369**, 850–854.